Old Dominion University
ODU Digital Commons

Electrical & Computer Engineering Faculty Publications

Electrical & Computer Engineering

1992

Effect of Magnetic and Density Fluctuations on the Propagation of Lower Hybrid Waves in Tokamaks

George Vahala

Linda L. Vahala
Old Dominion University, lvahala@odu.edu

Paul T. Bonoli

Follow this and additional works at: https://digitalcommons.odu.edu/ece_fac_pubs

Part of the Engineering Commons, Engineering Physics Commons, and the Plasma and Beam Physics Commons

Effect of magnetic and density fluctuations on the propagation of lower hybrid waves in tokamaks

George Vahala
Department of Physics, College of William & Mary, Williamsburg, Virginia 23185

Linda Vahala
Department of Electrical and Computer Engineering, Old Dominion University, Norfolk, Virginia 23529

Paul T. Bonoli
Plasma Fusion Center, Massachusetts Institute of Technology, Cambridge, Massachusetts 02139

Lower hybrid waves have been used extensively for plasma heating, current drive, and ramp-up as well as sawteeth stabilization. The wave kinetic equation for lower hybrid wave propagation is extended to include the effects of both magnetic and density fluctuations. This integral equation is then solved by Monte Carlo procedures for a toroidal plasma. It is shown that even for magnetic/density fluctuation levels on the order of 10^{-4}, there are significant magnetic fluctuation effects on the wave power deposition into the plasma. This effect is quite pronounced if the magnetic fluctuation spectrum is peaked within the plasma. For Alcator-C-Mod [I. H. Hutchinson and the Alcator Group, *Proceedings of the IEEE 13th Symposium on Fusion Engineering* (IEEE, New York, 1990), Cat. No. 89CH 2820-9, p. 13] parameters, it seems possible to be able to infer information on internal magnetic fluctuations from hard x-ray data—especially since the effects of fluctuations on electron power density can explain the hard x-ray data from the JT-60 tokamak [H. Kishimoto and JT-60 Team, in *Plasma Physics and Controlled Fusion* (International Atomic Energy Agency, Vienna, 1989), Vol. I, p. 67].

I. INTRODUCTION

There is much recent theoretical and experimental interest in the propagation of lower hybrid (LH) waves in tokamaks. In particular, LH waves have been utilized experimentally[1-8] for electron and ion plasma heating, for the sustainment and rampup of the toroidal plasma current, as well as in the stabilization of sawteeth. However, LH wave penetration is expected to be limited to the r/a >0.5 in a reactor due to the relatively high central electron temperatures and densities[9] $[T_e(0) \approx T_i(0) \gtrsim 25$ keV, $n_e(0) \gtrsim 1 \times 10^{14}$ cm^{-3}, and a is the minor plasma radius]. Nevertheless, LH current drive may be useful in the reactor regime in several applications dealing with current profile control. These applications[10,11] include current profile broadening to maintain magnetohydrodynamic (MHD) stability as well as in raising the on-axis safety factor to $q(0) \gtrsim 2$ in order to be able to access the second stability regime. Localized LH radio-frequency (rf) current generation may also be useful for the stabilization of sawteeth ($m=1$) instabilities in a tokamak reactor. Thus, an accurate determination of the LH-rf current density profile is important in accessing the feasability of each of these applications. Hence the importance of studying the effects of both magnetic and density fluctuations on the propagation and absorption of LH waves.

Most recent studies[12] of LH heating and current drive have used a one-dimensional radial transport code, coupled to a Fokker–Planck toroidal ray-tracing code. These computer models examine the confinement of the suprathermal electrons produced by LH current drive as well as the transport properties of the bulk electrons. Unfortunately, it is computationally prohibitive to incorporate into these codes the effects of scattering from fluctuations, even though it is well known[13] that fluctuations can play a major role on LH wave propagation, accessibility and absorption. Hence, here we shall concentrate on determining the effects of fluctuations on LH waves.

In Sec. II, the theory of Bonoli and Ott[13] is extended to now include the effects of magnetic fluctuations in the propagation of a wave packet through a toroidal plasma. This wave kinetic equation is then solved by Monte Carlo methods for LH wave propagation in Sec. III for Alcator-C-Mod[14] parameters. In Sec. IV, we connect up our wave scattering results to experimental hard x-ray data[15] from the JT-60 tokamak[16] and find that hard x-ray emission could give information on the level of internal magnetic fluctuations in Alcator-C-Mod. In Sec. V, we summarize our results.

II. WAVE KINETIC EQUATION WITH MAGNETIC AND DENSITY FLUCTUATIONS

The wave kinetic equation of Bonoli and Ott[13] considers wave scattering from density fluctuations only. Here, we extended this theory to also include the effects of scattering from magnetic fluctuations. From Maxwell's equations it is readily found,[17] on Fourier transforming the wave equation, that

$$\Lambda_{\alpha\beta}(\mathbf{k},\omega)E_\beta(\mathbf{k},\omega) = \sum_{\mathbf{k}',\omega'} \Bigg([\delta_{\alpha\beta} - \epsilon_{\alpha\beta}(\mathbf{k}',\omega')]$$

$$\times \frac{\delta n(\mathbf{k}-\mathbf{k}',\omega-\omega')}{N_0} + \frac{i\omega_{ce}\omega'}{\omega_{pe}^2}[\delta_{\alpha\gamma}$$

$$-\epsilon_{\alpha\gamma}(\mathbf{k},\omega)]e_{\gamma\rho\kappa}[\delta_{\rho\beta} - \epsilon_{\rho\beta}(\mathbf{k}',\omega')]$$

$$\times \frac{\delta B_\kappa(\mathbf{k}-\mathbf{k}',\omega-\omega')}{B_0} \Bigg) E_\beta(\mathbf{k}',\omega'), \quad (1)$$

where $\epsilon_{\alpha\beta}$ is the standard plasma dielectric tensor, and $\Lambda_{\alpha\beta}(\mathbf{k},\omega)$ is defined by

$$\Lambda_{\alpha\beta}(\mathbf{k},\omega) = (c^2/\omega^2)(k_\alpha k_\beta - k^2 \delta_{\alpha\beta}) + \epsilon_{\alpha\beta}(\mathbf{k},\omega), \quad (2)$$

where δn and $\delta\mathbf{B}$ are the density and magnetic fluctuations, ω_{ce} is the electron gyrofrequency, and ω_{pe} is the electron plasma frequency. Here, N_0 and $\mathbf{B}_0$ are the equilibrium density and magnetic field. Also, $\delta_{\alpha\beta}$ is the Kronecker symbol, and $e_{\gamma\rho\kappa}$ is the standard Levi-Citiva symbol: $+1$ for proper rotation of unrepeated subscripts, -1 for improper rotation of unrepeated subscripts, and 0 for repeated subscripts. Summation over repeated subscripts is understood.

If there were no fluctuations, Eq. (1) would reduce to

$$\Lambda_{\alpha\beta}(\mathbf{k},\omega_k)E_\beta(\mathbf{k},\omega_k) = 0, \quad (3)$$

so that a wave would propagate as a normal mode in the plasma with frequency $\omega = \omega_k$, determined by the dispersion relation

$$\det|\Lambda_{\alpha\beta}(\mathbf{k},\omega_k)| = 0. \quad (4)$$

If the density and magnetic fluctuations are sufficiently small, one can assume that the effects of the fluctuations on the wave propagation can be determined perturbatively from the normal mode propagation:

$$\omega = \omega_k + i\frac{\partial}{\partial t}, \quad \text{with} \quad \left|\frac{\partial}{\partial t}\right| \ll \omega_k. \quad (5)$$

Substituting Eq. (5) into Eq. (1) and introducing the unit polarization vector $\mathbf{e}(\mathbf{k})$

$$\mathbf{E}(\mathbf{k}) \equiv \mathbf{e}(\mathbf{k})E(\mathbf{k}), \quad (6)$$

one finds, on contracting the resulting equation with the polarization vector $e_\alpha^*(\mathbf{k})$,

$$ie_\alpha^*(\mathbf{k})\frac{\partial\Lambda_{\alpha\beta}}{\partial\omega}e_\beta(\mathbf{k})\frac{\partial E(\mathbf{k})}{\partial t}$$

$$= \sum_{\mathbf{k}'}\Bigg(e_\alpha^*(\mathbf{k})[\delta_{\alpha\beta}-\epsilon_{\alpha\beta}(\mathbf{k})]\frac{\delta n(\mathbf{k}-\mathbf{k}')}{N_0} + \frac{i\omega_{ce}\omega}{\omega_{pe}^2}e_\alpha^*(\mathbf{k})$$

$$\times[\delta_{\alpha\gamma}-\epsilon_{\alpha\gamma}(\mathbf{k})]e_{\delta\rho\kappa}[\delta_{\rho\beta}$$

$$-\epsilon_{\rho\beta}(\mathbf{k}')]\frac{\delta B_\kappa(\mathbf{k}-\mathbf{k}')}{B_0}\Bigg)e_\beta(\mathbf{k}')E(\mathbf{k}'). \quad (7)$$

In deriving Eq. (7), the frequency shift $\omega \to \omega'$ introduced by the fluctuations is neglected since it is a second-order effect: Typically, the fluctuation frequency spectrum of interest is below 1 MHz, while the incident electromagnetic wave frequencies are above 1 GHz.

Following Bonoli and Ott,[13] one now introduces the wave energy density

$$u(\mathbf{k}) \equiv \frac{\omega_k}{8\pi}e_\alpha^*(\mathbf{k})\frac{\partial\Lambda_{\alpha\beta}}{\partial\omega}e_\beta(\mathbf{k})|E(\mathbf{k})|^2 \quad (8)$$

and the wave amplitude

$$C(\mathbf{k}) = |u(\mathbf{k})|^{1/2}, \quad (9)$$

so that, from Eq. (7), we can derive the time evolution of $C(\mathbf{k})$:

$$i\frac{\partial C(\mathbf{k})}{\partial t} = \sum_{\mathbf{k}'}\Bigg(V^n(\mathbf{k},\mathbf{k}')\frac{\delta n(\mathbf{k}-\mathbf{k}')}{N_0}$$

$$+ V_\alpha^B(\mathbf{k},\mathbf{k}')\frac{\delta B_\alpha(\mathbf{k}-\mathbf{k}')}{B_0}\Bigg)C(\mathbf{k}'). \quad (10)$$

Here, V^n is the (scalar) density coupling coefficient and is defined by

$$V^n(\mathbf{k},\mathbf{k}')$$

$$\equiv -\frac{\omega_k}{2}\frac{e_\alpha^*(\mathbf{k})[\epsilon_{\alpha\beta}(\mathbf{k})-\delta_{\alpha\beta}]e_\beta(\mathbf{k}')}{[e_\gamma(\mathbf{k})M_{\gamma\kappa}e_\kappa(\mathbf{k})]^{1/2}[e_\mu(\mathbf{k}')M_{\mu\nu}e_\nu(\mathbf{k}')]^{1/2}}. \quad (11)$$

Here, $\mathbf{V}^B$ is the (vector) magnetic coupling coefficient

$$V_\alpha^B(\mathbf{k},\mathbf{k}') \equiv -\frac{i\omega_{ce}\omega_k^2}{2\omega_{pe}^2}$$

$$\times\frac{e_\beta^*(\mathbf{k})[\epsilon_{\beta\theta}(\mathbf{k})-\delta_{\beta\theta}]e_{\lambda\theta\alpha}[\epsilon_{\lambda\tau}(\mathbf{k}')-\delta_{\lambda\tau}]e_\tau(\mathbf{k}')}{[e_\gamma(\mathbf{k})M_{\gamma\kappa}e_\kappa(\mathbf{k})]^{1/2}[e_\mu(\mathbf{k}')M_{\mu\nu}e_\nu(\mathbf{k}')]^{1/2}}, \quad (12)$$

with the tensor $M_{\alpha\beta}$ being defined by

$$M_{\alpha\beta} \equiv \frac{1}{2}\omega_k\frac{\partial\Lambda_{\alpha\beta}}{\partial\omega}. \quad (13)$$

Assuming weak turbulence,[18] a wave kinetic equation can be derived from Eq. (10) in the random phase approximation by treating the coupling coefficients as small parameters. In the continuum limt, with the wave energy density

$$u(\mathbf{k}) \to F(\mathbf{x},\mathbf{k},t), \quad (14)$$

we find

4034   Phys. Fluids B, Vol. 4, No. 12, December 1992

Vahala, Vahala, and Bonoli   4034

$$\left(\frac{dF}{dt}\right)_{\text{ray}} = 2\pi \int d^2k'_{\perp} \, [F(\mathbf{x},\mathbf{k}',t) - F(\mathbf{x},\mathbf{k},t)]$$

$$\times \delta(\omega_{k'} - \omega_k)[S^n(\mathbf{k}-\mathbf{k}')\,|\,V^n(\mathbf{k},\mathbf{k}')\,|^2$$

$$+ S^B_{\alpha\beta}(\mathbf{k}-\mathbf{k}')\,|\,V^B_\alpha(\mathbf{k},\mathbf{k}')V^B_\beta(\mathbf{k},\mathbf{k}')\,|^2 + \dots]. \quad (15)$$

The density wave-number spectral density $S^n(\mathbf{k}-\mathbf{k}')$ is the continuum limit of $|\delta n(\mathbf{k}-\mathbf{k}')/N_0|^2$, and the corresponding magnetic spectral density $S^B_{\alpha\beta}(\mathbf{k}-\mathbf{k}')$ is the continuum limit of $|\delta B_\alpha(\mathbf{k}-\mathbf{k}')\delta B_\beta(\mathbf{k}-\mathbf{k}')/B_0^2|$. Both spectral densities have a slowly varying spatial dependence due to the inhomogeneous toroidal equilibrium. The omitted terms in Eq. (15), represented by ..., arise from the density-magnetic cross correlation. These effects are weak and can be neglected. Finally, $(dF/dt)_{\text{ray}}$ is the time evolution of the wave energy density following a ray trajectory in the toroidal tokamak equilibrium, allowing for wave damping due to resonant particle electron Landau damping, resonant particle ion Landau damping as well as electron-electron and electron–ion collisional damping

$$\left(\frac{dF}{dt}\right)_{\text{ray}} \equiv \left(\frac{dF}{dt}\right)_r + 2\gamma(\mathbf{x},\mathbf{k})F(\mathbf{x},\mathbf{k},t), \quad (16)$$

where $(dF/dt)_r$ is the conservative Lagrangian derivative following the ray.

In deriving the integral kernel of Eq. (15), it has been assumed that during the wave scattering off the fluctuations both the wave frequency ω_k and wave parallel wave number $k_{\parallel}$ are conserved. This approximation is valid provided the frequency and parallel wave number of the fluctuations are sufficiently smaller than ω_k and $k_{\parallel}$ —and this is well satisfied for the particular case studied here: the scattering of lower hybrid waves by magnetic and density fluctuations. During the scattering process the perpendicular wave number $\mathbf{k}_{\perp}$ is rotated through an angle β with

$$\mathbf{k}_{\perp} \cdot \mathbf{k}'_{\perp} = k_{\perp} k'_{\perp} \cos\beta. \quad (17)$$

The magnitudes of $\mathbf{k}_{\perp}$ and $\mathbf{k}'_{\perp}$ are determined from the respective wave dispersion relation, with both like-mode and unlike-mode scattering being permitted (slow → fast or slow wave, fast → fast or slow wave).

It is convenient[13] in evaluating the integrals in Eq. (15) to transform from the polar coordinates $(k'_{\perp}, \phi')$ to (κ, β) with

$$\beta = \phi' - \phi, \quad \kappa = |\mathbf{k}'_{\perp} - \mathbf{k}_{\perp}|, \quad (18)$$

so that the wave kinetic equation reduces to

$$\left(\frac{dF}{dt}\right)_{\text{ray}} = \frac{2\pi k_{\perp}}{V_g} \int_0^\infty d\kappa \, \delta(\kappa - \kappa_w) k'_{\perp} \int_0^{2\pi} d\beta [F(\phi+\beta)$$

$$- F(\phi)][S^n(\kappa)\,|\,V^n(k_{\perp},\kappa,\beta)\,|^2$$

$$+ S^B_{\alpha\beta}(\kappa)\,|\,V^B_\alpha(k_{\perp},\kappa,\beta)V^B_\beta(k_{\perp},\kappa,\beta)\,|\,], \quad (19)$$

where V_g is the group velocity perpendicular to $\mathbf{B}_0$: $V_g = -\partial\omega_{k'}/\partial k'_{\perp}$, $\kappa_w = |\mathbf{k}_{\perp} - \mathbf{k}'_{\perp}|$ with $\mathbf{k}_{\perp}$ and $\mathbf{k}'_{\perp}$ determined from the local dispersion relation. Here, $S^n(\zeta)$ is the perpendicular density fluctuation wave-number spectrum. This is related to the mean-square density fluctuations by

$$\left\langle \left(\frac{\delta n}{N_0}\right)^2 \right\rangle \equiv 2\pi \int_0^\infty d\zeta \, \zeta S^n(\zeta). \quad (20)$$

Since little is known about the structure of internal tokamak magnetic fluctuations, we assume for simplicity an isotropic magnetic spectrum perpendicular to $\mathbf{B}_0$ with

$$\left\langle \frac{\delta B_\alpha \, \delta B_\beta}{B_0^2} \right\rangle \equiv 2\pi \int_0^\infty d\zeta \, \zeta S^B_{\alpha\beta}(\zeta). \quad (21)$$

For like-mode scattering [i.e., slow → slow wave, or fast → fast wave], Eq. (19) readily simplifies since in this case $k_{\perp} = k'_{\perp}$, and $\kappa = 2k_{\perp} \sin\beta/2$:

$$\left(\frac{dF}{dt}\right)_{\text{ray}} = \frac{2\pi k_{\perp}}{V_g} \int_0^{2\pi} d\beta [F(\phi+\beta) - F(\phi)]$$

$$\times \left[S^n\left(2k_{\perp}\sin\frac{\beta}{2}\right)|\,V^n(k_{\perp},\beta)\,|^2 \right.$$

$$\left. + S^B_{\alpha\beta}\left(2k_{\perp}\sin\frac{\beta}{2}\right)|\,V^B_\alpha(k_{\perp},\beta)V^B_\beta(k_{\perp},\beta)\,| \right]. \quad (22)$$

Thus during like-mode scattering, the magnitude $\mathbf{k}_{\perp}$ remains invariant but its direction is rotated through an angle β. The coupling coefficients V^n and $\mathbf{V}^B$ are weighted by the corresponding wave-number spectra $S^n(\kappa)$ and $\mathbf{S}^B(\kappa)$ whose argument κ is just that needed for momentum conservation: $\kappa = \mathbf{k}'_{\perp} - \mathbf{k}_{\perp}$. Similarly for unlike-mode scattering (slow → fast wave, or fast → slow wave), except that now the scattered magnitude $k'_{\perp\sigma}$ acquires that value determined by the dispersion relation for that scattered mode (here σ refers either to the final unlike-mode, either a slow or fast wave). Again, this scattering process can only occur provided there is momentum conservation, $\kappa_\sigma = \mathbf{k}'_{\perp\sigma} - \mathbf{k}_{\perp}$. Thus the final wave kinetic equation (19) can be written in the form

$$\left(\frac{dF}{dt}\right)_{\text{ray}} = \sum_{\sigma=s,f} \int_0^{2\pi} d\beta [F(\phi+\beta) - F(\phi)]$$

$$\times [S^n(\kappa_\sigma)K^n(k'_{\perp\sigma},k_{\perp},\beta)$$

$$+ S^B_{\alpha\beta}(\kappa_\sigma)K^B_{\alpha\beta}(k'_{\perp\sigma},k_{\perp},\beta)], \quad (23)$$

where we make explicit the possible mode conversion process by the summation over σ, with $\sigma=s,f$ denoting the slow and fast wave roots of the dispersion relation, and

$$K^n(k'_{\perp\sigma},k_{\perp},\beta) \equiv \frac{2\pi k'_{\perp\sigma}}{V_{g\sigma}}\,|\,V^n(k'_{\perp\sigma},k_{\perp},\beta)\,|^2, \quad (24)$$

$$K_{\alpha\beta}^B(k'_{\perp\sigma},k_\perp,\beta) \equiv \frac{2\pi k'_{\perp\sigma}}{V_{g\sigma}} \mid V_{\alpha\beta}^B(k'_{\perp\sigma},k_\perp,\beta) \mid^2. \quad (25)$$

Monte Carlo solution to the wave kinetic equation, Eq. (23). Now $F(\phi+\beta)$ in Eq. (23) corresponds to the increase in the wave energy density $F(\phi)$ due to the scattering of waves at $\phi+\beta$ into ϕ. On the other hand, the $F(\phi)$ term in Eq. (23) corresponds to the attenuation in the wave energy density $F(\phi)$ due to wave scattering. Let $P(\beta)d\beta\,dt$ be the probability of scattering through an angular interval $(\beta,\beta+d\beta)$ in time dt. From Eq. (23), we see that

$$P(\beta) = \sum_{\sigma=s,f} [S^n(\kappa_\sigma)K^n(k'_{\perp\sigma},k_\perp,\beta) \\ + S_{\alpha\beta}^B(\kappa_\sigma)K_{\alpha\beta}^B(k'_{\perp\sigma},k_\perp,\beta)]; \quad (26)$$

i.e.,

$$P(\beta) \equiv \sum_{\sigma=s,f} P_\sigma(\beta), \quad (27)$$

where the $P_\sigma(\beta)$ are defined in Eq. (26).

The Monte Carlo integration of the wave kinetic equation proceeds as follows.[13]

(a) Choose a time Δt such that the total probability of all scattering through any angle, p, is small

$$p = \Delta t \sum_{\sigma=s,f} \int_0^{2\pi} d\beta\, P_\sigma(\beta) \equiv p_S + p_F \ll 1. \quad (28)$$

(b) Using a toroidal ray-tracing code, the position of the wave packet is advanced by integrating Eq. (16) over this time interval Δt. During the time Δt, multiple scattering events are avoided [since $p \ll 1$, Eq. (28)], and energy deposition into the plasma is calculated from the term $2\gamma F$ in Eq. (16).

(c) The effects of the fluctuations are now taken into account by a Monte Carlo procedure. Suppose the wave is a slow wave before scattering. Generate a random number X_r from a uniform probability distribution on the interval [0,1]. With p_S and p_F defined in Eq. (28),

if $0 \leqslant X_r < p_S \Rightarrow$ like-mode scattering: slow→slow wave,

if $p_S \leqslant X_r < p_S$

$\qquad + p_F \Rightarrow$ unlike-mode scattering: slow→fast wave,

$$(29)$$

if $X_r > p_S + p_F \Rightarrow$ no scattering.

(d) If it is determined that no scattering occurs in step (c) then one goes to (b).

(e) If scattering is to occur, then denote the scattered wave is σ [determined according to Eq. (29)]. The random scattering angle β is then generated from the distribution

$$G_\sigma(\beta) = \frac{P_\sigma(\beta)}{\int_0^{2\pi} d\beta\, P_\sigma(\beta)}. \quad (30)$$

Finally, the scattered wave number $\mathbf{k}'$ is determined from Eq. (17), with $\mid k'_\perp \mid$ being determined from the appropriate wave dispersion relation and $k_\parallel$ being fixed during the scattering process (c), (e). Explicitly, in standard toroidal coordinates, $\mathbf{k} \to \mathbf{k}'$ with[13]

$$k'_\phi = k_\parallel b_\phi + \frac{k'_\perp}{k_\perp} [(k_\phi - k_\parallel b'_\phi)\cos\beta + (k_\theta b_r \\ - k_r b_\theta)\sin\beta],$$

$$k'_\theta = \frac{b_r(k_\perp k'_\perp \cos\beta + k_\parallel^2) - k_r k_\parallel - k'_\phi(k_\phi b_r - k_r b_\phi)}{k_\theta b_r - k_r b_\theta},$$

$$(31)$$

$$k'_r = \frac{k_\parallel - k'_\theta b_\theta - k'_\phi b_\phi}{b_r},$$

and $\mathbf{b}$ is the unit vector in the direction of the magnetic field

$$\mathbf{b} = \mathbf{B}/\mid \mathbf{B} \mid. \quad (32)$$

An energy deposition profile can thus be determined for one particular realization of the random scattering process by iterating on steps (b)–(e) until a prescribed amount of wave absorption occurs (in the calculations reported here, the iterations are stopped after 99% of the initial wave energy is absorbed by the plasma). The average energy deposition profile is obtained after performing J realizations of the random scattering process. In the limit $J \to \infty$, $\Delta t \to 0$, a Monte Carlo solution to the wave kinetic equation (23) is obtained.

It is important to note that while $k_\parallel$ is conserved during the scattering process itself, steps (c) and (e), $k_\parallel$ will be modified by both toroidal effects and magnetic shear during the integration step (b).

III. LOWER HYBRID WAVE SCATTERING

A. Lower hybrid wave propagation

On including both electromagnetic and warm plasma effects, the local plasma dispersion relation for LH wave propagation is given by[19]

$$D_0(\mathbf{x},\mathbf{k},\omega) = p_6 n_\perp^6 + p_4 n_\perp^4 + p_1^2 n_\perp^2 + p_0 = 0. \quad (33)$$

The coefficient p_6 arises from thermal effects

$$p_6 = -\frac{3\omega_{pi}^2}{\omega^2}\frac{v_{\mathrm{th}\,i}^2}{c^2} - \frac{3\omega_{pe}^2}{4\omega_{ce}^2}\frac{\omega^2\rho_e^2}{c^2}, \quad (34)$$

and gives rise to the ion plasma wave branch. Here, $v_{\mathrm{th}\,i}$ is the ion thermal speed and ρ_e is the electron gyroradius.

The slow and fast wave branches arise from the quartic terms in Eq. (33) with the coefficients

$$p_4 = \epsilon_\perp ,$$

$$p_2 = (\epsilon_\perp + \epsilon_\parallel)(n_\parallel^2 - \epsilon_\perp) + \epsilon_{ij}^2, \qquad (35)$$

$$p_0 = \epsilon_\parallel [(n_\parallel^2 - \epsilon_\perp)^2 - \epsilon_{ij}^2],$$

where $\epsilon_\perp$ and $\epsilon_\parallel$ are elements of the cold plasma dielectric tensor perpendicular and parallel to the magnetic field, and for $\omega_{ci}^2 \ll \omega^2 \ll \omega_{ce}^2$,

$$\epsilon_\perp \approx 1 + \frac{\omega_{pe}^2}{\omega_{ce}^2} - \frac{\omega_{pi}^2}{\omega^2}, \quad \epsilon_\parallel \approx 1 - \frac{\omega_{pe}^2}{\omega^2} - \frac{\omega_{pi}^2}{\omega^2}$$

and ϵ_{ij} are the x-y cross terms (with the local magnetic field in the z direction)

$$\epsilon_{ij} \approx \omega_{pe}^2 / \omega\omega_{ce} .$$

The parallel and perpendicular refractive wave indices are defined by

$$n_\parallel = ck_\parallel / \omega, \quad n_\perp = ck_\perp / \omega. \qquad (36)$$

While the toroidal ray-tracing code will automatically handle the question of accessibility of the LH wave into the plasma, it seems appropriate to give the theoretically determined bounds on the parallel wave number for LH wave propagation

$$n_a(r) < n_\parallel < n_{eld}(r). \qquad (37)$$

Here, $n_a(r)$ is the Stix–Golant lower limit[20]

$$n_a(r) = \frac{N_0^{1/2}(r)}{B_0} + \left[1 + N_0(r) \left(\frac{1}{B_0^2} - \frac{0.44}{K(\omega/2\pi)^2} \right) \right]^{1/2}, \qquad (38)$$

where the magnetic field B_0 is in Tesla, the electron density $N_0(r)$ in 10^{13} cm^{-3}, $\omega/2\pi$ in GHz and $K = N_i Z_i^2 m_p / N_0 m_i$. Here, Z_i is the ion charge (of mass m_i and density N_i) and m_p is the proton mass. The upper limit, $n_{eld}(r)$, is determined by heavy electron wave Landau damping

$$n_{eld}(r) = [A/T_e(r)]^{1/2}, \qquad (39)$$

where the coefficient A has been determined from numerical computations[20,21]

$$A = 50, \quad \text{electron Landau damping,}$$

$$A = 60\text{–}80, \quad \text{quasilinear (plateau) wave damping.} \qquad (40)$$

TABLE I. Typical tokamak parameters.

	Alcator-C-Mod	JT-60
Minor radius, a	21.0 cm	93.0 cm
Vacuum wall radius	23.7 cm	106.0 cm
Major radius	67.0 cm	300.0 cm
Toroidal current	3.0 MA	1.0 MA
Toroidal magnetic field	9.0 T	4.0 T
LH wave frequency	4.6 GHz	2.0 GHz
Central electron density	3.5×10^{14} cm^{-3}	1.5×10^{13} cm^{-3}
Central electron and ion temperature	5.0 keV	2.0–3 keV
$n_\parallel$ of incident LH wave	2.0	1.29, 1.93, 2.88

B. LH wave scattering from density and magnetic fluctuations

We now examine the effects of density and magnetic fluctuations on lower hybrid wave propagation. To be specific, we consider wave propagation in an Alcator-C Mod-like deuterium plasma with parameters given in Table I. The details of the model toroidal tokamak equilibrium can be found in Ref. 13 and so will not be presented here.

From experimental data,[22] it has been determined that the density fluctuation spectrum $S^n(\zeta)$ is well approximated by a Gaussian

$$S^n(\zeta) = \frac{1}{\pi \zeta_0^2} \left\langle \left(\frac{\delta n}{N_0} \right)^2 \right\rangle \exp\left(-\frac{\zeta^2}{\zeta_0^2} \right). \qquad (41)$$

Here, ζ_0^{-1} is the correlation length of the density fluctuations, and the spatial density fluctuation profile is assumed to be peaked at the plasma edge and has the form

$$\left[\left\langle \left(\frac{\delta n}{N_0} \right)^2 \right\rangle \right]^{1/2} \equiv a_n \exp\left[-b_n \left(\frac{r}{a} - 1 \right)^2 \right]. \qquad (42)$$

Here, a_n and b_n are parameters defined in Table II, and a is the plasma radius.

On the otherhand, there is little experimental data on internal magnetic fluctuations in hot tokamaks. For simplicity, we shall assume that the magnetic fluctuation

TABLE II. Fluctuation parameters.

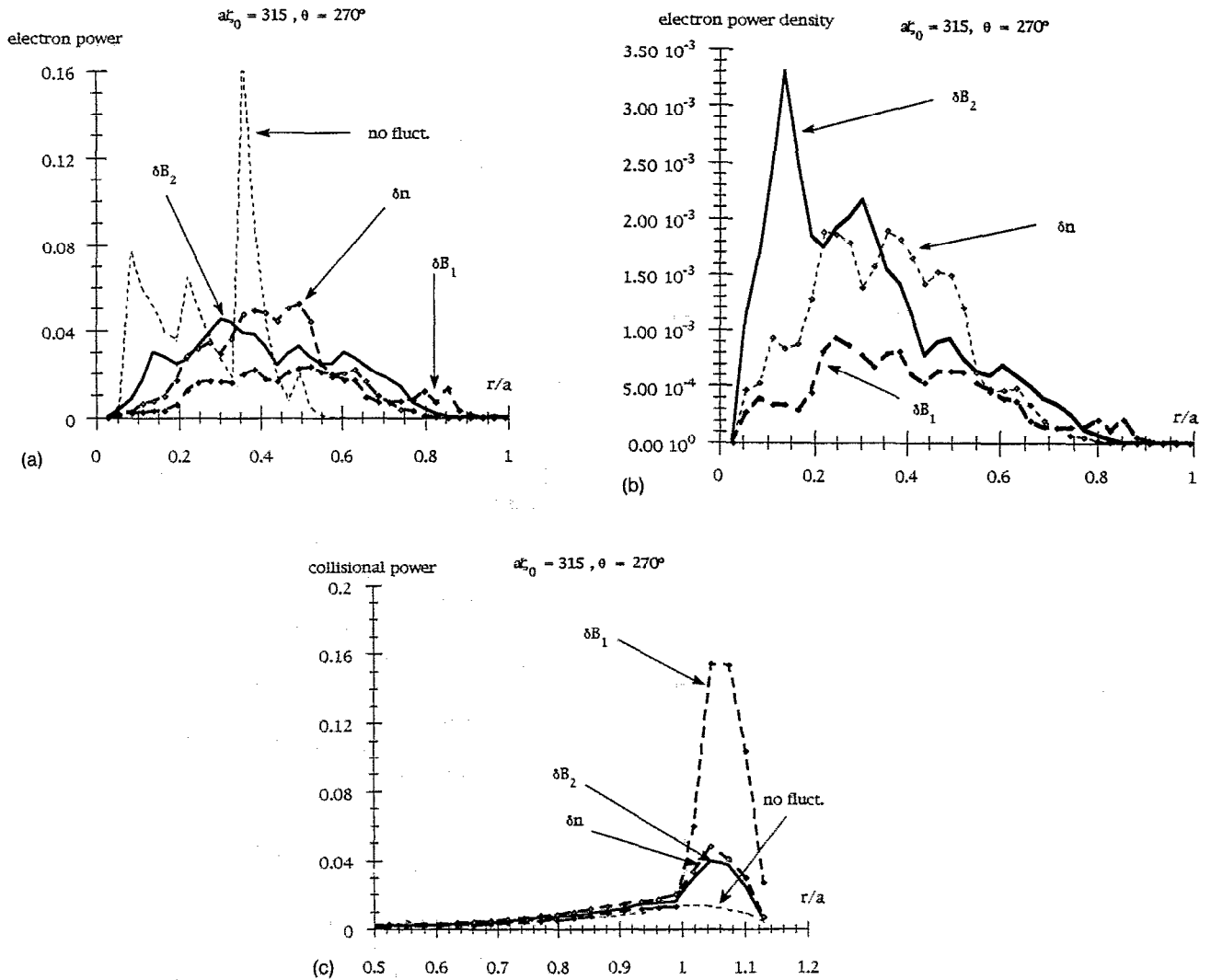|	Density fluctuations δn	Density + magnetic fluctuations δB_1	Density + magnetic fluctuations δB_2
Amplitude	$a_n = 0.333$	$a_b = 0.333 \times 10^{-2}$	$a_b = 0.333 \times 10^{-2}$
Form factor	$b_n = 272.25$	$b_b = 272.25$	$b_b = 272.25$
Peak in spatial profile	$r = a$	$r_b = a$	$r_b = 0.6a$
Correlation length	$a\zeta_0 = 315$	$a\zeta_{0B} = 315$	$a\zeta_{0B} = 315$
or	$a\zeta_0 = 157$	$a\zeta_{0B} = 157$	$a\zeta_{0B} = 157$
Poloidal launch	$\theta = 0°$	$\theta = 0°$	$\theta = 0°$
position or	$\theta = 270°$	$\theta = 270°$	$\theta = 270°$

FIG. 1. Radial plasma absorption of an incident LH wave with $\omega/2\pi = 4.6$ GHz, launched from the bottom of the cross section ($\theta = 270°$) with refractive index $n_\parallel = 2.0$ into an Alcator-C-Mod plasma (see Table I). (a) Electron power, (b) electron power density, and (c) collisional power deposition profiles for an. The cross section is partitioned into 41 equally spaced radial bins and the vertical axis units are (a), (c) MW/bin per 1 MW incident wave for power deposition; and (b) MW cm^{-3}/bin per 1 MW incident wave for power density deposition—i.e., the power density deposition profiles are just the power in each bin/bin volume. The dashed curves are the profiles assuming no plasma fluctuations. The δn curves (dashed curves with open diamonds) are the profiles for 10% edge density fluctuations with spectral properties listed in Table II. The δB_1 curves (dashed curves with closed diamonds) are the profiles for 10% edge density fluctuations and edge magnetic fluctuation levels down by 10^{-4} from that of the density fluctuations, Eq. (46). The δB_2 curves (solid curve) are similar to the δB_1 curves, except now the magnetic fluctuations are peaked internally within the plasma at $r/a = 0.6$. The fluctuation spectra are assumed to have a correlation wave number of 15 cm^{-1}, so that $\zeta_0 a = 315$. There is substantial difference in the δB_2 and δB_1 curves, which is must apparent in the power density profiles, (b). There is also strong collisional loss if edge magnetic fluctuations are present, (c). The truncated peak in the δB_1 profile arises from the somewhat coarse grid of 41 radial bins.

wave-number spectrum perpendicular to $\mathbf{B}_0$ is isotropic and also given by a Gaussian

$$S_{\alpha\alpha}^B(\zeta) = \frac{1}{\pi \zeta_{0B}} \left\langle \frac{\delta B_\perp^2}{B_0^2} \right\rangle \exp\left(-\frac{\zeta^2}{\zeta_{0B}^2} \right). \tag{43}$$

Here, ζ_{0B}^{-1} is the perpendicular correlation length of the magnetic fluctuations. The spatial magnetic fluctuation profile is assumed to have a similar form to Eq. (42):

$$\left(\left\langle \frac{\delta B_\perp^2}{B_0^2} \right\rangle \right)^{1/2} \equiv a_b \exp\left[-b_b \left(\frac{r}{r_b} - 1 \right)^2 \right], \tag{44}$$

where the parameters a_b, b_b, and r_b are specified in Table II. Typically, density fluctuations are peaked at the plasma

edge but it is believed that magnetic fluctuations may be more peaked in the plasma interior rather than at the edge. Hence, we will consider two specific spatial magnetic fluctuation profiles:

case δB_1: magnetic fluctuation spectrum peaked at the edge: $rb = a$,

case δB_2: internal magnetic fluctuation spectrum peaked at $rb = 0.6a$, (45)

and their effects on LH wave propagation.

We shall consider the average power density deposited to the electrons as a function of radius for poloidal launch angle $\theta = 270°$ (rays launched from the bottom of the tokamak) or $\theta = 0°$ (rays launched from the low-field side).

Averages are performed over 100 Monte Carlo iterations and the radial power density deposition is calculated by dividing the plasma cross section into 41 radial shells and determining the power per unit volume in each radial shell. It will sometimes be convenient to consider the electron power profile—this is just the power absorbed by the electrons in a given radial shell. The ray paths are followed by integrating the wave kinetic equation, Eq. (23), until 99% of the incident wave power has been deposited into the plasma. For the particular parameters under discussion here, we find negligible power deposition to the ions while there can be substantial collisional power loss near the plasma edge.

First consider a poloidal launch angle $\theta = 270°$ and a perpendicular correlation wave number of 15 cm^{-1}. This is typical of the correlation lengths detected in Alcator-A. Thus $\zeta_0 a = 315$. For simplicity, we shall assume a similar magnetic fluctuation correlation length. In Fig. 1(a), we plot the radial electron power deposition, and the corresponding power density in Fig. 1(b). From Fig. 1(a), we see that fluctuations tend to broaden out the power over most of the cross section. Moreover, from Fig. 1(b), it is evident that more power density is deposited to the central electrons if internal magnetic fluctuations are present—case δB_2—as compared to both the absence of magnetic fluctuations—case δn—or if the magnetic fluctuations are peaked at the plasma edge—case δB_1. Note also that there is substantially more collisional losses if magnetic fluctuations are present and peaked at the plasma edge, Fig. 1(c). It should be remembered that in all our calculations the strength of magnetic to density fluctuations is assumed to be

$$\frac{\langle \delta B_1^2 \rangle / B_0^2}{\langle \delta n^2 \rangle / N_0^2} = 10^{-4}, \quad (46)$$

a level that seems reasonable and possibly detectable experimentally by microwave scattering[23] in hot tokamaks.

The effect of longer fluctuation correlation lengths on lower hybrid wave propagation at $\theta = 270°$ is considered in Fig. 2. If only density fluctuations were present (δn), then there is a strong enhancement of electron power density deposition near the center. This is clearly seen by comparing Figs. 1(b) and 2. There is no longer a pronounced difference when magnetic fluctuations are present or if the magnetic fluctuation spectrum is peaked internally (δB_2) or at the edge (δB_1). Moreover, the longer correlation lengths lead to a lower collisional power loss at the plasma edge by about a factor of 3.

In Fig. 3, we consider LH wave propagation for an initial ray angle of $\theta = 0°$ for 15 cm^{-1} fluctuation correlation wave number. If there were no fluctuations in the plasma we find a very strong enhancement in central electron power deposition for initial ray angle $\theta = 0°$ over that for $\theta = 270°$, cf. Figs. 3(a) and 1(a). This strong enhancement is destroyed by plasma fluctuations. There is also a marked difference in both electron and collisional power deposition depending on whether the magnetic fluctuations are peaked at the edge (δB_1) or peaked internally (δB_2).

On the other hand, there is no significant difference between the case of just density fluctuations (δn) and that in which there are also internal magnetic fluctuations (δB_2) present together with these density fluctuations [Fig. 3(b)].

If the fluctuation correlation length is doubled for initial ray angle of $\theta = 0°$, Fig. 4, then the difference in power density deposition due to magnetic fluctuations peaked at the edge, δB_1, and those peaked internally, δB_2, and where they are peaked is diminished. This was also the case for initial ray angle of $\theta = 270°$ and a correlation wave number of 7.5 cm^{-1} (Fig. 2).

C. Validity of the Monte Carlo solution

We shall first consider the effects of the size of our ensemble in solving the wave kinetic equation, Eq. (23). Figures 1–4 were determined from averages over 100 Monte Carlo samples. We have run the case $a\zeta_0 = 315$ (i.e., correlation wave number of 15 cm^{-1}) and initial ray angle $\theta = 270°$ for 500 Monte Carlo iterations and present the statistical comparisons in Fig. 5. This case was chosen because of the strong effect on power deposition of magnetic fluctuations peaked internally at $r/a = 0.6$ over that where the magnetic fluctuations were peaked at the plasma edge, $r/a = 1.0$. We conclude from Fig. 5 that the results discussed in Sec. III are not an artifact of the ensemble size but are indicative of the effect of weak magnetic fluctuations on lower hybrid wave propagation—even for peak magnetic to density fluctuations of

$$\frac{\langle \delta B_1^2 \rangle / B_0^2}{\langle \delta n^2 \rangle / N_0^2} = 10^{-4}.$$

The wave kinetic equation, Eq. (23), has been derived assuming weak turbulence theory. In particular, the random phase approximation requires that the scattering cor-
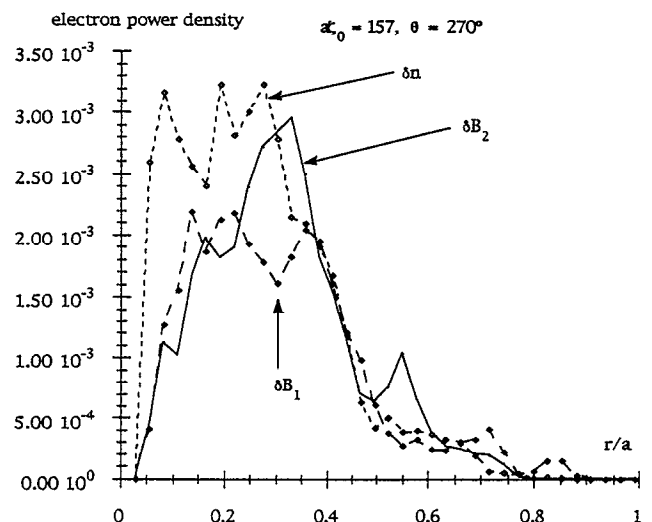

FIG. 2. The effect of decreasing the fluctuation correlation wave number from 15 to 7.5 cm^{-1} on the electron power density profiles. There is a substantial reduction in the collisional power loss in the δB_1 curve by a factor of 3.

electron power $a t_0 = 315, \theta = 0°$

(a)

electron power density $a t_0 = 315, \theta = 0°$
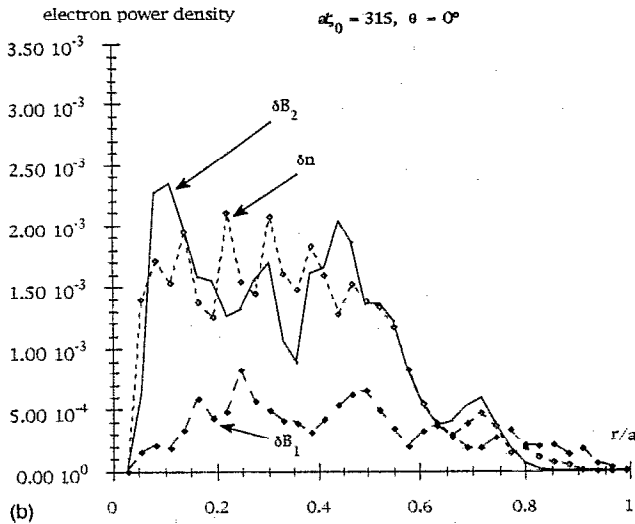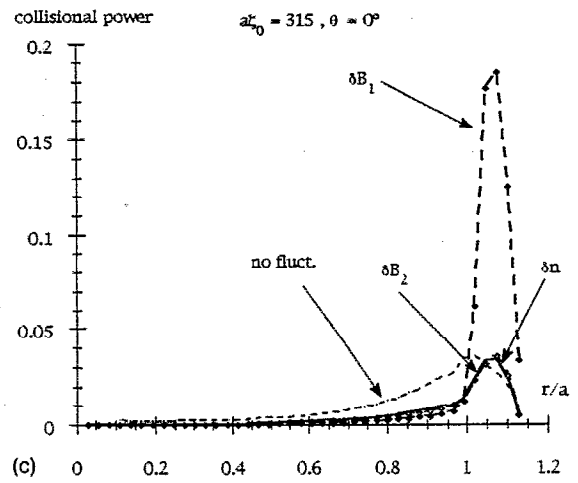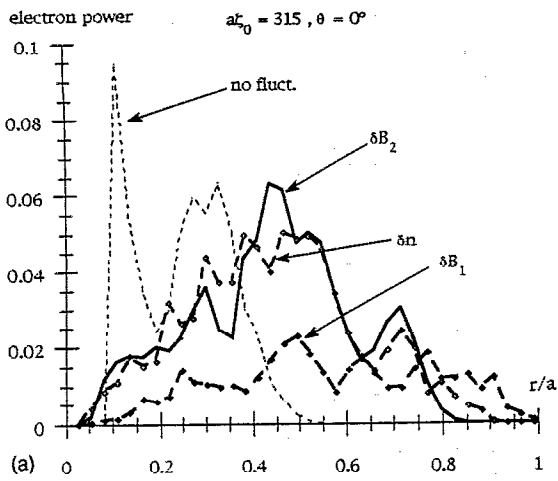
(b)

collisional power $a t_0 = 315, \theta = 0°$

(c)

FIG. 3. Radial plasma absorption of an incident LH wave with $\omega/2\pi$ = 4.6 GHz, launched from the low field side ($\theta = 0°$) with refractive index $n_\parallel = 2.0$ and fluctuation correlation wave number of 15 cm^{-1} into an Alcator-C-Mod plasma (see Table I). (a) Electron power, (b) electron power density, and (c) collisional power deposition profiles. Note that if there were no fluctuations, the electron power is strongly absorbed near the plasma center, (a), while fluctuations broaden the electron power substantially. There is little difference whether one has internal magnetic fluctuations superimposed on the density fluctuations or not, as evidenced from the power density profiles δB_2 and δn in (b). There is substantial difference between edge and internal magnetic fluctuations, δB_1 and δB_2 curves in (b). Again, there is substantial collisional power loss, (c), when there are edge magnetic fluctuations present.

relation wavelength, λ_{corr}, exceeds the fluctuation correlation wavelength, ζ_0^{-1}:

$$\lambda_{\mathrm{corr}} > \zeta_0^{-1}. \tag{47}$$

Here, λ_{corr} can be related[13] to the scattering length λ_s, which is defined to be the distance the wave must propagate in order that its wave vector $\mathbf{k}_\perp$ be rotated through angle of 90°. Here, λ_s is determined in the following way[13] (we present the details for like-mode scattering, but one proceeds in the same way for unlike-mode scattering): in Eq. (22), one notices that the ray-tracing Lagrangian time derivative is a linear operator in ϕ on the wave energy density F

$$\left(\frac{dF}{dt}\right)_{\mathrm{ray}} \equiv L_\phi[F], \tag{48}$$

so that

$$F[\phi] = \cos p\phi, \quad p = 0,1,2,... \tag{49}$$

is an eigenfunction of the wave kinetic equation (22), with eigenvalue-ν_p
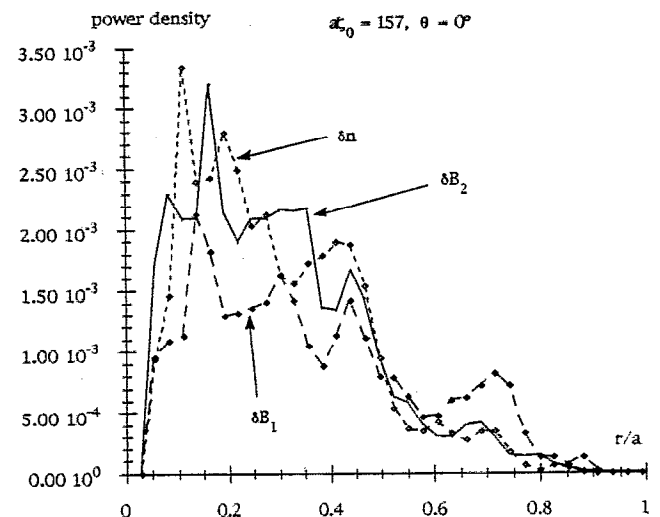
power density $a t_0 = 157, \theta = 0°$

FIG. 4. The effect of doubling the fluctuation correlation length on the electron power density for the situation of Fig. 3. The results are similar to those when the ray is launched from the bottom of the cross section, Fig. 2.
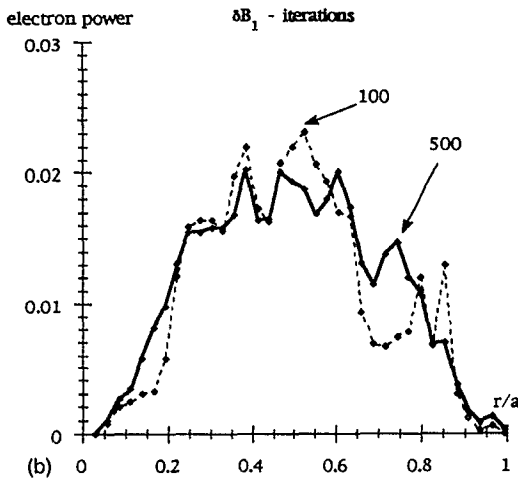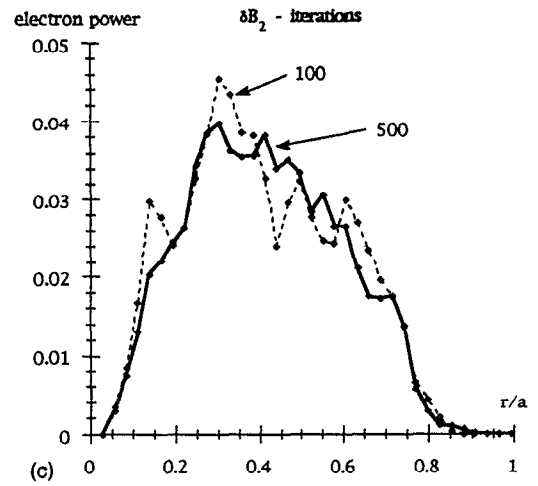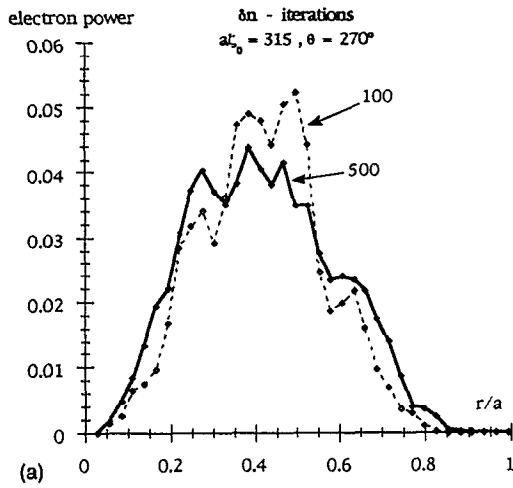
FIG. 5. The effect of the number of Monte Carlo iterations in the solution of the wave kinetic equation (23) for the parameters of Fig. 1 for edge density fluctuations (a), edge density and edge magnetic fluctuations (b), and edge density and internal magnetic fluctuations (c). The dashed curves are for 100 iterations, while the solid curves are for 500 iterations.

$$\nu_p = \frac{4\pi k_\perp}{V_g} \int_0^{2\pi} d\beta \, \sin^2\left(\frac{p\beta}{2}\right)$$

$$\times \left[S^n\left(2k_\perp \sin\frac{\beta}{2}\right) |V^n(k_\perp,\beta)|^2 \right.$$

$$\left. + S^B_{\alpha\beta}\left(2k_\perp \sin\frac{\beta}{2}\right) |V^B_\alpha(k_\perp,\beta) \, V^B_\beta(k_\perp,\beta)| \right]. \quad (50)$$

Since

$$\left(\frac{dF}{dt}\right)_{\text{ray}} = L_\phi(\cos p\phi) = -\nu_p \cos p\phi, \quad (51)$$

ν_p can be thought of as the damping[13] due to scattering of the pth harmonic of the wave energy density F. A scattering length λ_s can then be defined as the lowest-order directional component of F (namely $p=1$)

$$\lambda_s = V_g/\nu_1 . \quad (52)$$

Ott,[24] using the direct interaction approximation (DIA)[25] to the wave scattering problem, has shown that the use of the random phase approximation in weak turbulence theory is valid provided

if $k_\perp \gg \zeta_0$: $\lambda_s\left(\dfrac{\zeta_0}{k_\perp}\right)^2 > \zeta_0^{-1}$ or $\lambda_{\text{corr}} \approx \lambda_s\left(\dfrac{\zeta_0}{k_\perp}\right)^2$,

if $k_\perp \ll \zeta_0$: $\lambda_s > \zeta_0^{-1}$ or $\lambda_{\text{corr}} \approx \lambda_s$,   (53)

on using Eq. (47). Typically, it has been found[13] that the conditions Eq. (53) are violated near the slow–fast wave mode conversion point since in this region $V_g \to 0$, i.e., $\lambda_s \to 0$. However, the divergence of the scattering probability is logarithmic at this point and so we have introduced a numerical cutoff procedure in which the right hand side of Eq. (23) is set to zero when $\lambda_s < \lambda_{\text{corr}}$.

IV. FLUCTUATIONS AND HARD X-RAY INTENSITY MEASUREMENTS

During LH current drive, the wave parameters are so chosen that the launched waves can be absorbed by the electrons. The electron distribution function will then develop a very energetic suprathermal tail. The collisions of these suprathermal electrons with the bulk plasma ions gives rise to a continuum of bremsstrahlung radiation in the form of hard x rays.[26] These hard x rays are readily detected experimentally. In particular, for the JT-60 tokamak (see Table I for the relevant parameters) Uehara et al.[15] have obtained experimental data on the dependence
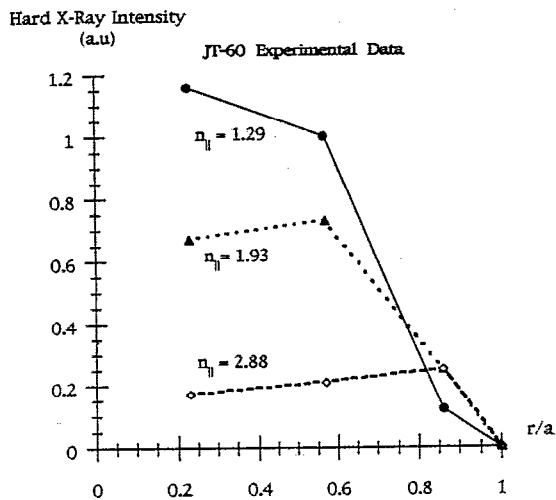
FIG. 6. JT-60 hard x-ray intensity measurements at four chordal positions for the parameters listed in Table I. Since an Abel inversion had to be performed, there is some uncertainty in the actual radial position of these x-ray data points.

FIG. 8. The effect of the parameter b_n on the spatial density fluctuation profile. Figures 1–4 have used the sharp fluctuation profile $b_n = 272.25$.

of the radial hard x-ray emission spectra on the *initial* $n_\parallel$ of the launched LH wave. The data[15] are from three radial chord positions for each such $n_\parallel$, Fig. 6, after Abel transforms are performed on the emission signals.

If one assumes no density or magnetic fluctuations then the right-hand side of Eq. (23) is zero. Equation (23) is then readily integrated to give the power density deposition profile to the electrons. It should be noted that it is the electron power density deposition profile that is more correlated to the hard x-ray data rather than the volume-integrated power profile. For the parameters corresponding
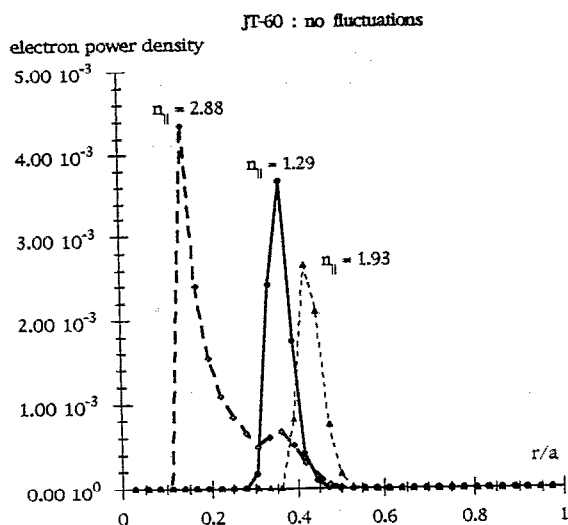
to the experimental data, Fig. 6, and assuming no fluctuations, the electron power density deposition profiles are shown in Fig. 7. Even allowing for a time lapse in which some spatial diffusion of the suprathermal electrons occurs before the emission of hard x rays from the bremsstrahlung collisions, it is still very difficult to correlate Fig. 7 with Fig. 6—especially for the case of incident LH wave with initial $n_\parallel = 2.88$.

To obtain electron power density profiles that resemble the hard x-ray data, we broadened the spatial density fluctuation prfile, Eq. (42), by decreasing b_n from $b_n = 272.25$ to $b_n = 68$. The resultant effect on the normalized spatial density fluctuation profile $\langle \delta n^2 \rangle / N_0^2$ is shown in Fig. 8. The corresponding electron power density deposition profile is

FIG. 7. Theoretical electron power density profiles for the same JT-60 parameters as in Fig. 6, for $n_\parallel = 1.29$, $n_\parallel = 1.93$, and $n_\parallel = 2.88$, if there were no plasma fluctuations. These density deposition profiles (especially that for $n_\parallel = 2.88$) are quite different from the experimental hard x-ray data profiles, Fig. 6.
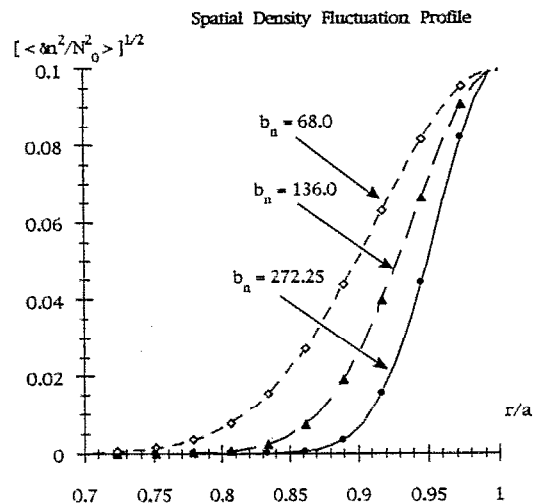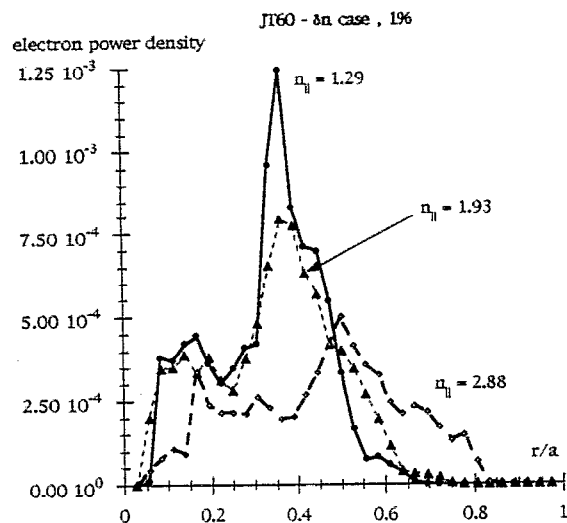

FIG. 9. The electron power density profiles determined from the wave kinetic equation with 1% edge density fluctuations with broad spatial density profile parameter $b_n = 68$. These profiles should be compared to the experimental hard x-ray data, Fig. 6. This level of density fluctuations can be achieved if the tokamak is run in a *divertor* mode.
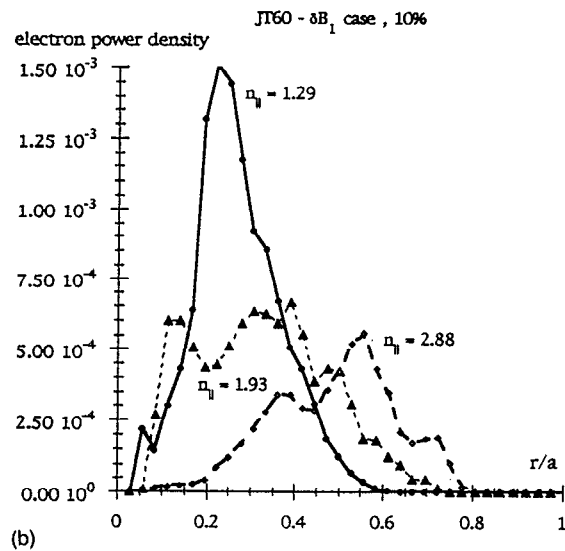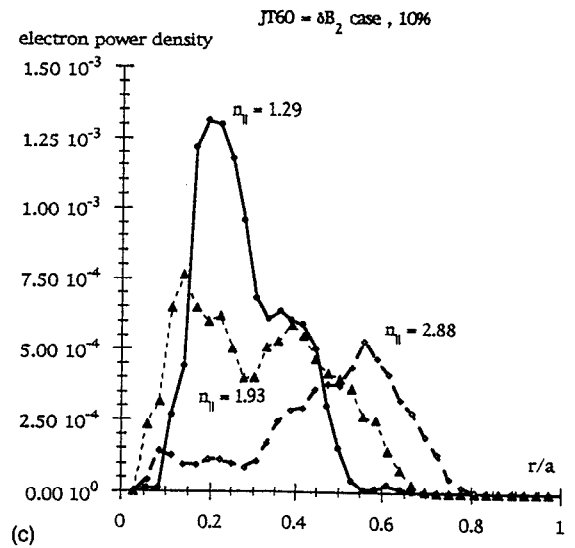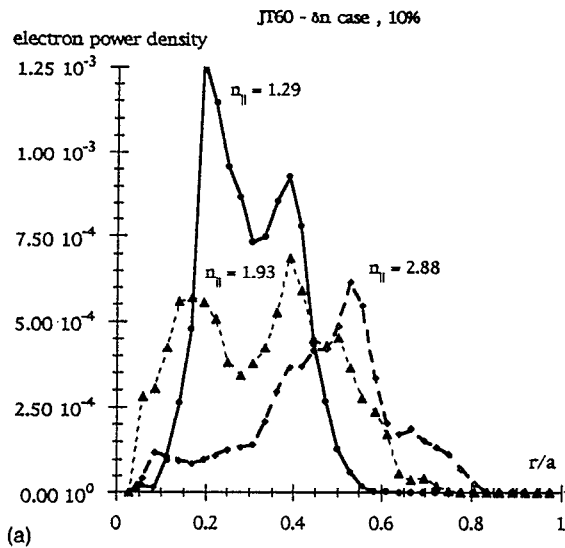
FIG. 10. The electron power density profiles for 10% edge density fluctuations: (a) only density fluctuations, δn, with spatial width $b_n = 68$, (b) edge density and edge magnetic fluctuations, δB_1, with spatial widths $b_n = b_b = 68$, (c) edge density and internal magnetic fluctuations, δB_2, with spatial widths $b_n = b_b = 68$. This level of density fluctuations is typical of tokamaks run in the limiter mode and the level of magnetic/density fluctuations is 10^{-4}. Note the strong correlation between the experimental results, Fig. 6, and the power density profiles (a).

shown in Fig. 9 for initial LH wave $n_{\parallel} = 1.29$, 1.93, and 2.88 with 1% edge density fluctuations. This low level of edge density fluctuations could be achieved if the tokamak was run in the divertor mode. While there is now better agreement with hard x-ray data over the case of no fluctuations, we find much better agreement if the plasma has a 10% edge density fluctuation level. This higher level of fluctuations is characteristic of tokamaks run in a limiter mode. With this level of density fluctuations, and neglecting magnetic fluctuations, the corresponding electron power density deposition profiles are shown in Fig. 10(a). Keeping in mind that the experimental hard x-ray data is determined from an Abel inversion with its accompanying fuzziness in spatial resolution, we see excellent agreement with the experimental curves. If there are also some edge magnetic fluctuations present at the level specified by Eq. (46), the δB_1 case, we obtain density profiles shown in Fig. 10(b), while if the magnetic fluctuations are peaked internally, the δB_2 case, the electron power density deposition profile is shown in Fig. 10(c).

For Alcator-C-Mod plasmas, with the tokamak run in the limiter mode and 10% edge density fluctuations, the corresponding electron density deposition profiles have al-

ready been given for $n_{\parallel} = 2.0$ [see Figs. 1(b), 2, 3(b), and 4]. If Alcator-C-Mod is run in the divertor mode and so achieves 1% edge density fluctuations, then Figs. 11 give the corresponding electron power density deposition profiles for initial $n_{\parallel} = 2.0$, 2.25, and 2.5. The profiles are plotted for four cases: only edge density fluctuations [δn case], edge density and edge magnetic fluctuations with $b_b = 272.25$ [δB_1 case, and Eq. (44)], and edge density and internal magnetic fluctuations with either $b_b = 272.25$ [δB_2 case] or with a broadened magnetic fluctuation profile $b_b = 68.0$ (δB_2^* case). From Fig. 11 one can readily conclude that hard x-ray profile measurements should be able to distinguish the δB_2^* case from the others. It is also possible that the dominant peaks near the plasma center, $r/a \approx 0.1$ (δB_1 case for $n_{\parallel} = 2.0$ and δn case for $n_{\parallel} = 2.5$), should be also distinguishable from hard x-ray emission.

V. CONCLUSIONS

We have extended the wave kinetic approach of Bonoli and Ott[13] to now include the effects of both magnetic and density fluctuations on LH wave propagation in toroidal geometry. The effects of fluctuations on LH wave propa-
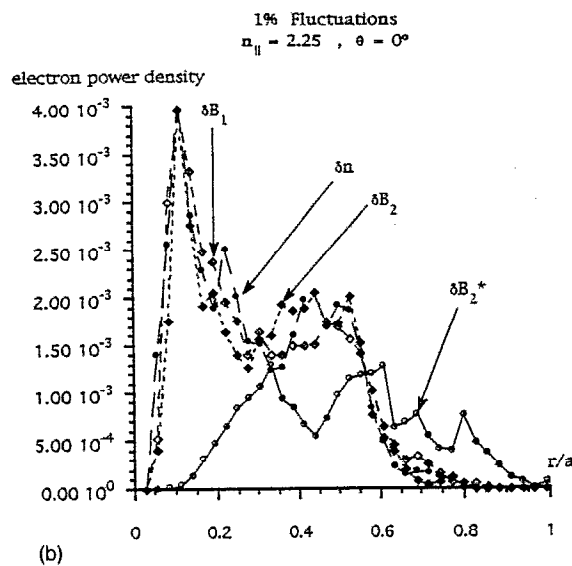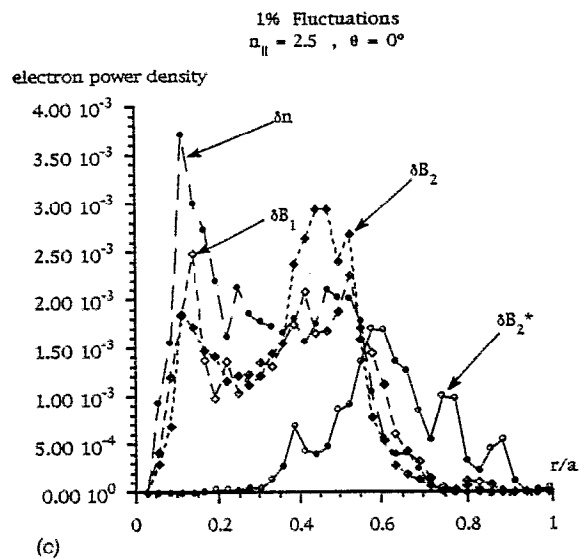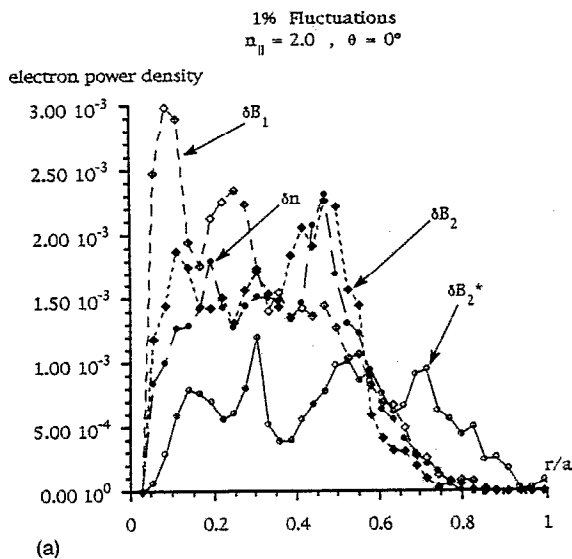
1% Fluctuations
$n_{||} = 2.0$, $\theta = 0°$

electron power density

(a)

1% Fluctuations
$n_{||} = 2.5$, $\theta = 0°$

electron power density

(c)

1% Fluctuations
$n_{||} = 2.25$, $\theta = 0°$

electron power density

(b)

FIG. 11. Electron power density profiles for Alcator-C-Mod parameters: LH wave frequency $\omega/2\pi = 4.6$ GHz with poloidal launch angle $\theta = 0°$ and (a) $n_{||} = 2.0$, (b) $n_{||} = 2.25$, (c) $n_{||} = 2.5$. In all cases, the relative strength of the magnetic to density fluctuations is 10^{-4}. δn case (solid curve): 1% edge density fluctuations, δB_1 case (open diamonds): 1% edge density fluctuations with peaked ($b_b = 272.25$) edge magnetic fluctuations, δB_2 case (solid diamonds): 1% edge density fluctuations with peaked ($b_b = 272.25$) internal magnetic fluctuations, δB_2^* case (open circles): 1% edge density fluctuations with broad ($b_b = 68$) edge magnetic fluctuations.

gation, accessibility and absorption are particularly important since LH waves are expected to play a major role in current ramp-up, current profile control, stabilization of $m = 1$ sawteeth instabilities as well as plasma heating. The results reported here can be viewed as complimentary to the standard LH wave studies in which a one-dimensional radial transport code is coupled to a Fokker–Planck toroidal ray-tracing code. In these transport studies, fluctuation effects are necessarily excluded since the addition of the Monte Carlo code to solve the wave kinetic equation would render these studies computationally prohibitive.

The hard x-ray data from JT-60 is analyzed and interpreted as giving direct information on the fluctuations in the plasma. It is expected, from the results reported here, that similar hard x-ray data on Alcator-C-Mod could give some information on the magnetic fluctuation spectrum. This, together with a recently proposed mode-conversion electromagnetic scattering diagnostic,[23] should give some insight on the level of internal magnetic fluctuations and aid in the establishment of the interconnection between fluctuations and transport.

[1] T. Yamanoto, T. Imai, M. Shimada, N. Suzuki, M. Maeno, S. Konoshima, T. Fujii, K. Uehara, T. Nagashima, A. Funahashi, and N. Fujisawa, Phys. Rev. Lett. **45**, 716 (1980).

[2] S. C. Luckhardt, M. Prokolab, S. F. Knowlton, K.-I. Chen, A. S. Fisher, F. S. McDermott, and M. Mayberry, Phys. Rev. Lett. **48**, 152 (1982).

[3] S. Bernabei, C. Daughney, P. Efthimion, W. Hooke, J. Hosea, F. Jobes, A. Martin, E. Mazzucato, E. Meservey, R. Motley, J. Stevens, S. Von Goeler, and R. Wilson, Phys. Rev. Lett. **49**, 1255 (1982).

[4] M. Porkolab, J. J. Schuss, B. Lloyd, Y. Takase, S. Texter, P. Bonoli, C. Fiore, R. Gandy, D. Gwinn, B. Lipschultz, E. Marmar, D. Pappas, R. Parker, and P. Pribyl, Phys. Rev. Lett. **53**, 450 (1984).

[5] C. C. Gormezano, P. Bibet, P. Blanc, P. Briand, G. Brifford, M. Clement, P. Grelot, W. Hess, G. Ichtchenko, G. Melin, B. Moulin, A. Panzarella, F. Parlange, E. Porrot, G. Rey, B. Taquet, F. Ternay, and D. Van Houtte, *Proceedings of the 11th European Cconference on Plasma*

Physis, Aachen, 1983 (European Physical Society, Petit-Lancy, 1983), p. 325.

[6]F. X. Soldner, K. McCormick, D. Eckhartt, M. Kornherr, F. Leuterer, R. Bartiromo, G. Becker, H. S. Bosch, H. Brocken, H. Derfler, A. Eberhagen, G. Fussmann, O. Gehre, J. Gernhardt, G. v. Gierke, A. Giuliana, E. Glock, O. Gruber, G. Haas, M. Hesse, J. Hofmann, A. Izvozchikov, G. Janeschitz, F. Karger, M. Keilhacker, O. Kluber, K. Lackner, M. Lenoci, G. Lisitano, F. Mast, H. M. Mayer, D. Meisel, V. Mertens, E. R. Muller, M. Munich, H. Murmann, H. Niedermeyer, A. Pietrzyk, W. Poschenrieder, H. Rapp, H. Riedler, H. Rohr, F. Ryter, K. H. Schmitter, F. Schneider, C. Setzensack, G. Siller, P. Smeulders, E. Speth, K.-H. Steuer, T. Vien, O. Vollmer, F. Wagner, F. v. Woyna, and D. Zasche, Phys. Rev. Lett. **57**, 1137 (1987).

[7]S. Knowlton, M. Porkolab, and Y. Takase, Nucl. Fusion **28**, 99 (1988).

[8]M. Porkolab, B. Lloyd, Y. Takase, P. Bonoli, C. Fiore, R. Gandy, R. Granetz, D. Griffin, D. Gwinn, B. Lipschultz, E. Marmar, S. McCool, A. Pachtman, D. Pappas, R. Parker, P. Pribyl, J. Rice, J. Terry, S. Texter, R. Watterson, and S. Wolfe, Phys. Rev. Lett. **53**, 1229 (1984).

[9]M. Brambilla, *Physics of Plasmas Close to Thermonuclear Conditions*, (Commission of European Community, Brussels, 1980), Vol. I, p. 291.

[10]M. J. Gerver, J. Kesner, and J. J. Ramos, Phys. Fluids **31**, 2674 (1988).

[11]P. T. Bonoli, M. Porkolab, J. J. Ramos, D. T. Blackfield, R. S. Devoto, and M. E. Fenstermacher, Nucl. Fusion **30**, 533 (1990).

[12]P. T. Bonoli, in *Applications of RF Power to Plasmas*, AIP Conf. Proc. 159 (American Institute of Physics, New York, 1987), p. 85

[13]P. T. Bonoli and E. Ott, Phys. Fluids **25**, 359 (1982).

[14]I. H. Hutchinson and the Alcator Group, *Proceedings of the IEEE 13th Symposium on Fusion Engineering*, edited by M. Lubell, M. Nestor, and S. Vaughan, Knoxville, 1990 (IEEE, New York, 1990), Cat. No. 89 CH 2820-9, p. 13.

[15]K. Uehara, H. Kimura, and JT-60 Team, in *Applications of RF Power to Plasmas*, AIP Conf. Proc. 190 (American Institute of Physics, New York, 1989), p. 106.

[16]H. Kishimoto and JT-60 Team, in *Plasma Physics and Controlled Fusion* (Internal Atomic Energy Association, Vienna, 1989), Vol. I, p. 67.

[17]A. G. Sitenko, *Electromagnetic Fluctuations in Plasma* (Academic, New York, 1967).

[18]R. Z. Sagdeev and A. A. Galeev, *Nonlinear Plasma Theory* (Benjamin, Reading, MA, 1969).

[19]T. H. Stix, Phys. Rev. Lett. **15**, 878 (1965).

[20]V. S. Belikov, Ya. I. Kolesnichenko, and I. S. Plotnik, Nucl. Fusion **31**, 827 (1991).

[21]P. T. Bonoli and M. Porkolab, Nucl. Fusion **27**, 1341 (1987).

[22]R. E. Slusher and C. M. Surko, Phys. Rev. Lett. **40**, 400 (1978); C. M. Surko and R. E. Slusher, Phys. Fluids **23**, 2425 (1980).

[23]L. Vahala, G. Vahala, and N. Bretz, Rev. Sci. Instrum. **61**, 3022 (1990); Phys. Fluids B **4**, 619 (1992).

[24]E. Ott, Phys. Fluids **22**, 1732 (1979).

[25]R. H. Kraichnan, J. Fluids Mech. **5**, 497 (1959).

[26]S. Texter, S. Knowlton, M. Porkolab, and Y. Takase, Nucl. Fusion **26**, 1279 (1986).